An Inkjet-Printed Artificial Neuron for Physical Reservoir Computing

Steven D. Gardner and Mohammad R. Haider
School of Engineering, University of Alabama at Birmingham, Birmingham, AL, USA
{stevendg, mrhaider}@uab.edu

***Abstract*—Inkjet printing circuits onto thin, flexible substrates is a newly explored field with respect to the transistor; a critical element needed to form logic gates and high-level active circuitry. The traditional approach is to achieve comparable performance to MOSFETs or BJTs. However, the introduction of neuromorphics, spintronics, memristors, chaotic materials and limitations of transistor sizes have incited a shift toward alternative computing schemes that do not behave as standard transistors. This work explores a minimal fabrication, low-cost, non-linear, current-controlled Graphene Inkjet Printed Artificial Neuron that performs the computing of a recurrent neural network when multiple units are coupled. An activation function (inverse hyperbolic sine) is fit to the electrical curve of the current-controlled Graphene element with R-Squared of 0.997. The standard neuron is replaced with the modeled one in the Echo State Network for training on the MNIST benchmark dataset for handwritten digit classification. Testing performance of the simulated inkjet printed neuron reached 88.1% classification, and was marginally better than the sigmoid and hyperbolic tangent functions. This work demonstrates a minimal-fabrication alternative computing element functioning as a simulated artificial neuron in the Echo State Network. Benefits include low-cost fabrication, high power-efficiency, physically flexible edge computing, and development into many applications within telehealth, infrastructure, military, sports, etc. This work supports efforts toward a printable, cost-effective, flexible, and scalable physical machine learning system.**

***Index Terms*—inkjet-printed circuits, graphene, reservoir computing, Echo State Network, alternative computing, physical computing**

I. Introduction

Silicon-based technology is the most well-established, rugged and reliable method of enabling access to high-frequency computing and ultimately the digital domain, of which society has come to rely on significantly. Decades-long efforts to industrialize the technology by reducing circuit and transistor dimensions have at last been met with physical limitations that effectively stunts innovations into the silicon transistor's evolution [1]. Achievements into the technology have cemented it as the industrial standard and has become a stepping stone toward alternative computing methods that perform in ways not capable with the existing archetypes. For instance, discoveries of physical, non-linear, chaotic elements are being researched for computing, with prominent ones including the memristor [2]–[4], spin transfer torque devices [5]–[7], quantum dot [8], and other non-traditional methods [9]–[11].

Many of those efforts are expensive, in their early phases of discovery, lack resources for commercialization, are not eco-friendly in their fabrication process, and/or have limitations of their own hindering widespread usage outside of the laboratories [12], [13]. Inkjet-printed (IJP) circuits is the fabrication approach used in this work, as it is suitable to overcome the need for non-linear, small dimension, power-efficient, eco-friendly, alternative computing that has the added benefit of flexibility such that it can be attached to non-uniform scenarios such as textiles, non-rigid objects, and curved/irregular surfaces. Furthermore, IJP technology is highly inexpensive, simple to design, instantly able to print new revisions rather than waiting months for CMOS fabrications, and can be printed using any home or office inkjet printer that is Drop-on-Demand and piezoelectric [14]. In the last 20 years, researchers have successfully used IJPs for laying conductive routing, leading to a plethora of sensors, antenna and Reservoir-Computing (RC) circuit designs [15]–[18]. Low-frequency IJP transistors that operate under the same mechanism of MOSFETs have also been made [19], [20], typically with high-precision equipment in a laboratory setting.

This work considers a minimal fabrication and low-cost IJP approach to non-linear, low-frequency computing. The device does not act as a standard MOSFET. Instead, its non-linearity can be utilized by attaching many units together, having it act as a neural network that linearly separates time-series data. The output signals of the neural network may then be interpreted by trained weights to give a classification of the input data [21]. In other words, many non-linear units together form a physical neural network compatible with the Echo State Network (ESN) [22], Liquid State Machine [23], and other systems [24], [25].

With IJP's many pros also comes with its cons, such as its inability to perform with high-frequency applications, uncertain fabrication reliability and repeatability, biasing sensitivity to nearby environmental conditions, and significant performance degradation after long-term usages. These challenges are minimized and considered within the contents of this work as developmental areas of improvement.

In this research, an IJP non-linear artificial neuron (IJPAN) is characterized and considered for usage within the ESN framework. First, an introduction is given for the modified ESN and its activation function dynamics (Section II and III). The IJPAN design/fabrication is explained with performance

results and computer aided modeling in Section IV. The modified ESN has its reservoir neuron type replaced to the modeled IJPAN function and is evaluated on the MNIST benchmark dataset (Section V). Results are discussed in Section VI and concluded with future work in Section VII.

II. ESN Architecture for Physical Reservoirs

The first reservoir computing network was created by H. Jaeger [22], [26], [27] with the Echo State Network (ESN) in 2001. The liquid state machine was separately invented at the same time by W. Maass in 2002 [23], [28], [29]. The Time Delay Reservoir was developed several years later [30], [31]. In each type of network the framework is the same: input data feeds into a "reservoir" that is a recurrent neural network that transforms the data into a high-dimension space, which can then be understood by training weights in machine learning algorithms. Details of the modified ESN used in this work was conducted and published in [32]. The standard ESN has a single reservoir of sparsely connected hyperbolic tangent activation functions that transform the input data into a hyperspace that is linearly separable and able to be interpreted by a linear read-out activation function (Eq. 1). Only the output layer is trained, according to a minimum cost gradient solution (i.e. least mean squares with ridge regularization), referred to as ridge regression (Eq. 2).

$$Y = W_{out} \times X \tag{1}$$

$$W_{out} = Y_{target} \times X^T (X \times X^T + \beta \times I)^{-1} \tag{2}$$

where:

Y = output classification
W_{out} = output weights
Y_{target} = desired output classification
X = state vector
β = regularization term
I = Identity matrix

A. Benchmark Dataset and mESN Prior Work

The MNIST benchmark dataset of handwritten digits [33] is used in this work to evaluate the performance of the proposed scheme. The dataset contains 60,000 handwritten images that have been size-normalized and centered in a fixed-size image of 28x28 pixels. Many neural networks have been tested with this established benchmark and some papers have examined the ESN with it, such as in [34] and [35]. Preliminary research showed that the modified ESN to classify the MNIST digits reached 95.3% classification with 1600 hyperbolic tangent functions [32]. This is an improvement to the standard ESN MNIST classification results of [34], where they achieve 90.5% with 1,200 activation functions, although they also reach above 98% classification by altering their output layer to use Multi-Layer Perceptrons. In [34], other recurrent neural networks are considered and show competitive classification rates of ESNs with the MNIST benchmark

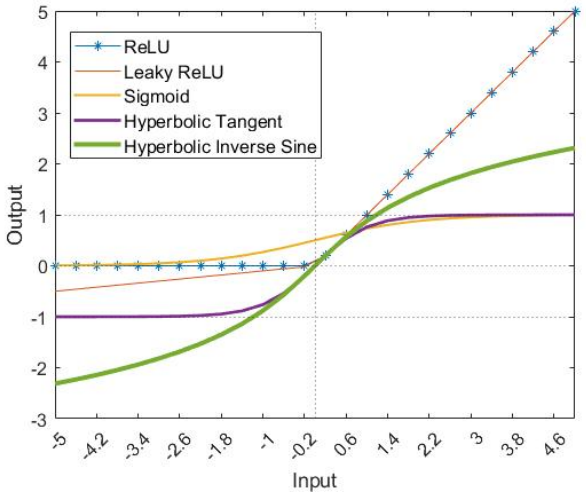

Fig. 1. Comparison of common activation functions, including ReLU, Leaky ReLU, Sigmoid, Hyperbolic Tangent, and Hyperbolic Inverse Sine. The sine function can be seen not saturating for large values, and is used in this work to model the behavior of the IJPANs.

starting at 93%. Highly-trained standard feed-forward neural networks have reached over 99%, but come with restrictions as to training time and computing power, mainly since all weights throughout the network must be updated during backpropagation. Data processing, performance metrics, and validation details of the mESN algorithm design for MNIST classification are included in [32] and support the efforts of this research.

III. Activation Functions for Machine Learning

Neural networks consist of artificial neurons (ANs), where each unit non-linearly transforms its input into a set range defined by a common function, referred to in this work as an activation, or squashing function. The most commonly used, as seen in Fig. 1 are sigmoid, hyperbolic tangent, and Rectified Linear Unit (ReLU), although several variations exist. A single AN cannot sufficiently perform linear separation on input data, which is an essential task required for machine learning. However, when many are connected as a network they can, forming a neural network that may then be trained. The same concept is applied with the modeled IJPAN of this work, where a network of simulated IJPANs performs the task needed to effectively train a learning algorithm.

The sigmoid function constrains the input to an output between [0,1], while the hyperbolic tangent has the same profile but squashes the input to [-1,1]. A limiting behavior of standard logistic sigmoid and hyperbolic tangent functions are that they saturate for large input values, making pattern recognition more challenging for dynamic time-series signals [36]. Variations of the hyperbolic function such as the inverse hyperbolic sine (Eq. 3) have similar non-linearity as the tangent and sigmoid, without saturation at high values. Preserving the transformation of large positive and negative inputs helps the algorithm converge during classification tasks [37]. For instance, the leaky ReLU is an adaptation to the standard ReLU where a small slope is given to the negative

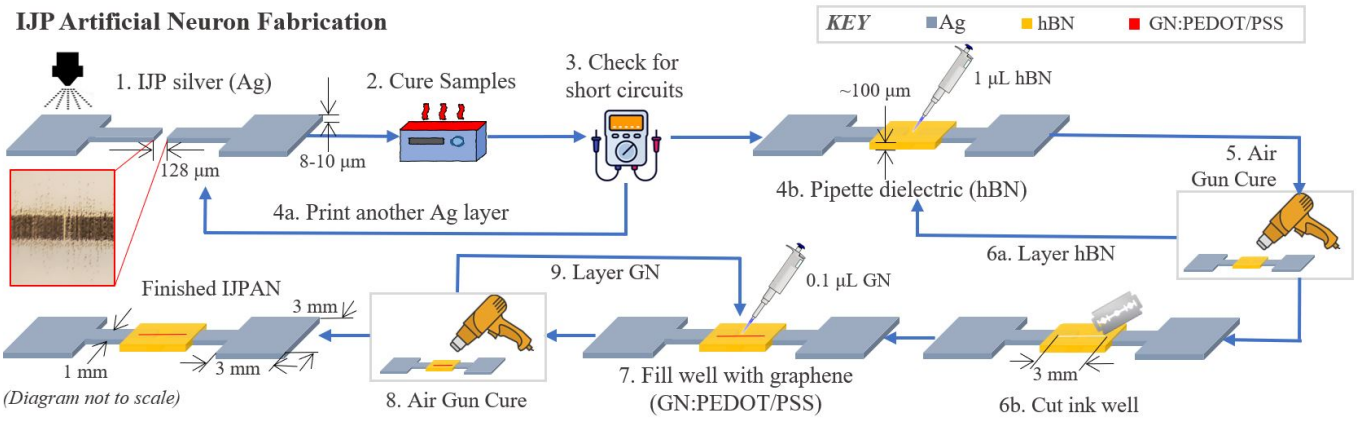

Fig. 2. The IJPAN fabrication process is shown along with the curing approaches and relevant dimensions. Multiple layers may be printed or deposited onto the substrate to ensure electrical properties such as maintaining open circuit at the channel region.

operating region. Information with negative input is then not entirely lost but preserved, while still containing non-linearity.

To summarize, the inverse hyperbolic sine function contains non-linearity, has comparable behaviors to the standard sigmoid and hyperbolic tangent functions, does not saturate for large input values, has no asymptotes, and is nearly identical to the behavior seen in the IJPAN. Therefore, it is used to model the behavior for signal biasing and computer-based experimental simulations.

IV. IJP Parallel Plate Non-Linear Element

As depicted in Fig 2, the artificial neuron is designed as silver (Ag) nanoparticle parallel plates printed onto polyethylene terephthalate (PET) film with a standard drop-on-demand, piezoelectric printer (Epson XP-960), followed by bridging the channel region between the parallel plates with graphene (GN/PEDOT:PSS) nanoparticle semiconductor ink, deposited via electronic pipette (1μL precision). First, silver parallel plates are printed with a gap of approximately 130 μm. The printer is rated for a minimum of 300 μm, and a significant amount of splattering is evident. However, this challenge is mitigated by orienting the gap along the moving axis of the print head, as the lateral movement causes the particle scattering imperfections. Conductivity is checked to ensure there is no shorting in the channel region.

Second, 1 μL of hexagonal Boron Nitride (hBN) is placed by pipette onto the channel (gap) region and cured at 150°C for 5 minutes until it sets completely. This material is a dielectric commonly used in IJP thin-film transistor designs, and serves to create an insulated canvas needed to control the channel region during the next steps. The coffee-ring effect, or the natural formation of high-concentration nanoparticles around the edge of the cured ink, is a critical flaw of IJP technology as it disrupts nanoparticle uniformity and makes reliability and repeatability more variable between samples. This research has found a method of mitigating that problem by cutting a well into the hBN across the gap, restricting the bounds with which the GN ink can spread and interact with the silver parallel plates. Thus, the next step to fabrication is using a sharp blade to cut into the hBN layer to form a well between terminals. A "Feather Dual Sided Blade" was sanitized and used to make the cut, and without applying too much pressure, the well is formed without damaging the PET substrate. The cutting process may be automated with the V-One PCB printer and will be considered in future work in repeatability and reliability studies. Lastly, the GN ink is dropped onto the well, which suctions into the cut space amid the cured hBN and avoids effects of the coffee-ring.

A. IJPAN Electrical CAD Model

The I-V curve of the IJPAN is shown in Fig. 3, where adding multiple layers of GN magnifies the amplitude while maintaining non-linearity. A voltage sweep was performed from -40V to +40V and back to -40V (repeated three times) to establish that the current does not shift, settle, or have hysteresis properties. A similar non-linear behavior seen here also occurs without the GN or hBN (i.e. only the silver terminals), although it is nearly imperceptible and appears linear at a distance. This is evidence of electron hopping between silver nanoparticles that are splattered during printing. Recent literature shows how hopping conduction induces I-V profile non-linearity and was used as an approach to analog

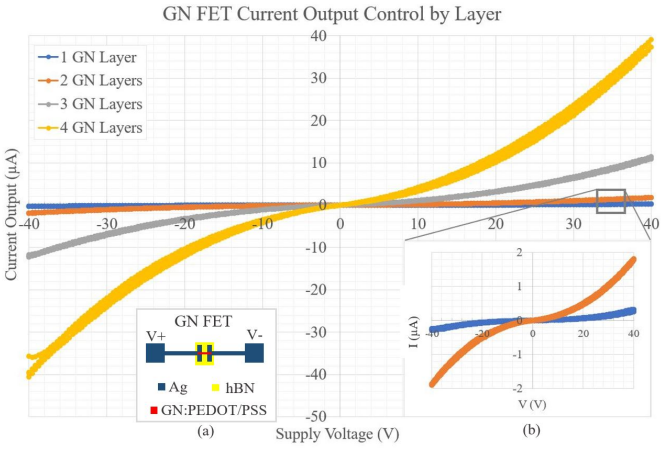

Fig. 3. The voltage-controlled I-V curve shows a behavior similar to the hyperbolic sine function. (a) A diagram of the fully fabricated element is shown. (b) A zoomed-in plot shows the same non-linear profile at lower amplitudes for when 1-2 layers of GN are placed. Adding layers of GN proportionately increases the output current for a given supply voltage.

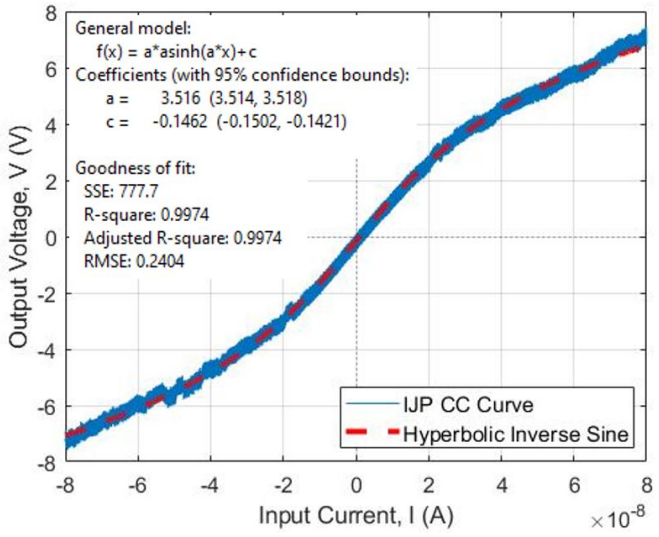

Fig. 4. The blue line shows the electrical response of the current-controlled GN IJPAN, where nano-amp current is input and voltage is output. The best fit model uses the inverse hyperbolic sine function (red dotted line).

neural networks [38]. Without the splattering or with widely separated terminals, the I-V curve is linear as defined by the conductivity of the substrate's gap between silver terminals (i.e. open circuit). Besides GN and silver, hBN is used which is a high-performance dielectric. Experimentation has shown that hBN reduces non-linearity with greater concentration, as it is restricting electron flow. The voltage-controlled curve follows a hyperbolic sine function, which has exponentially high outputs at large input values. The GN is causing most of the non-linearity, while silver splattering accounts for a small amount of the effect, and hBN dampens the non-linearity. The cause of graphene's non-linearity is determined to be trapped charge in the nanoparticles that gradually dissipates or discharges with higher applied energy. Greater concentrations of GN increase the total electron flow but still trap the charge, retaining its non-linearity.

A simple adjustment is then made where current is supplied, inducing a voltage across the terminals and giving the results shown in Fig. 4. This curve is proportional to the desired inverse hyperbolic sine function of Eq. 3.

$$Output = \alpha \times sinh^{-1}(\alpha \times Input) + C \tag{3}$$

where α and constant C define the biasing terms.

The least squares solution is shown in Eq. 4 and has an R-squared value of 0.997. This physical activation function is non-linear, differentiable, and does not saturate/explode at its limits, allowing information at the extremes not to be lost after activation (i.e. vanishing gradients are less common) [39].

$$V = 3.516 \times sinh^{-1}(3.516 \times |I|) - 0.1462 \tag{4}$$

where V and I represent the output voltage and input current, respectively. Thus, the GN IJPAN is a current-controlled device with a voltage output. The conductivity and power curves of the IJPAN can be visualized in Fig. 5. For linear I-V profiles, the conductivity plot is a flat line (shown by the red line). This helps to visualize the IJPAN non-linearity. The spikes near 0V are from the current's polarity change. The average power consumption is 108 μW per IJPAN.

Benefits of this module are that only nano-amps of current is needed to drive the IJPAN, the output can be biased for compatibility with a small micro-processor, reading voltage as an output eliminates the need for a analog-to-digital converter, and most importantly this overcomes the challenge most commonly seen in IJP technology, which is high voltage supply requirements. It is not unusual to see operating voltages between [-60, 60] V. Thus, by having the device be current-controlled, the output is a voltage that can be biased for compatibility with microprocessors. Furthermore, about 200 units can be printed on a single 11"x8.5" sheet of PET film, with multiple-paper routing for scaling. The IJPAN ESN in the following section has 200 ANs simulated as a recurrent neural network to classify handwritten digits from a benchmark dataset.

V. Simulated IJPAN Echo State Network

This section details the IJPAN replacement into the modified ESN (mESN), its operation, and results that are competitive with the standard AN types. First, the global parameters of the ESN are defined, followed by neuron replacement with the modeled equation (Eq. 4), and finally analysis of network error, activation performance, and algorithm processing time. The mESN algorithm as shown in Fig. 6, splits and distributes the data into multiple parallel reservoirs, in addition to data

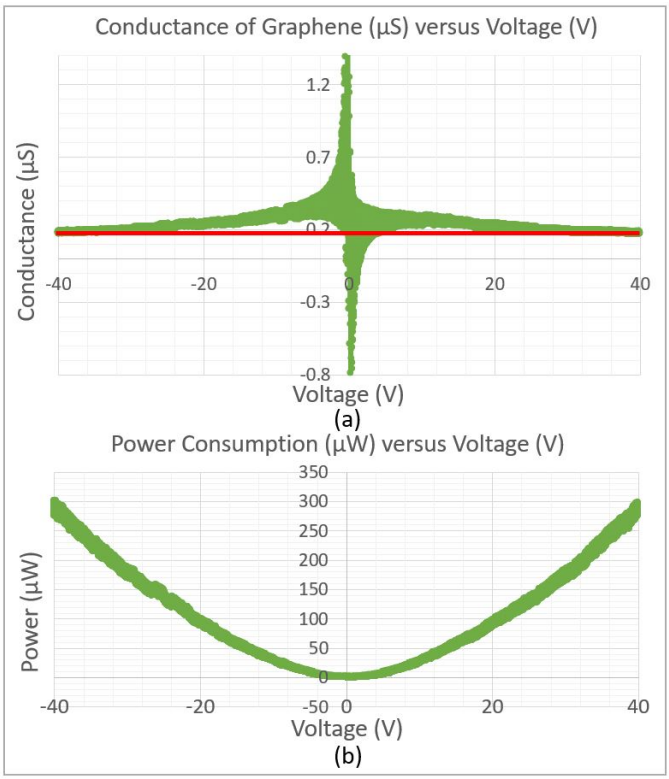

Fig. 5. Conductance and power curves. (a) Conductance curve clearly shows the non-linear deviations from the linear case, as noted by the horizontal red line. (b) Power curve shows the range of energy consumed per IJPAN element.

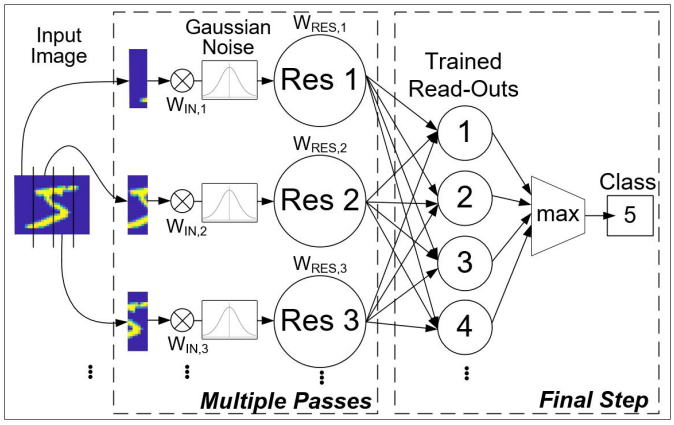

Fig. 6. A schematic of the modified ESN (mESN) architecture. The input image is split into equal parts and run through scaling, noise filter, and parallel reservoirs multiple times to allow for neuron convergence. The state vectors are joined and multiplied by the trained weights for each digit. The highest value of the readouts is considered the image's classification.

augmentation via noise injection for improved robustness. The hyperbolic tangent artificial neurons in the mESN are replaced with the modeled GN IJPAN as explored in this section.

A. IJPAN ESN Global Parameters

The modified ESN has many global parameters that define the system, with its performance depending strongly on what the values are initialized to before running the algorithm. As optimization is not within the scope of this work, a set of chosen parameters according to Table I have been used to generate the performance metrics of this work. The number of train/test samples in each epoch is split 80% train and 20% test. The added white Gaussian noise has signal-to-noise ratio of 10. These numbers are based on an understanding of the network dynamics and ability to perform quick evaluations from ultra-fast training times. The spectral radius is the maximum absolute eigenvalue of the reservoir's weights and identifies the memory of the system. A low spectral radius is expected for signals exhibiting low non-linearity (e.g., discrete images), and is further explored in [40] and [41]. A spectral radius less than 1 helps to ensure a stable framework. The pixels are already normalized to unity and scaling down the input weights will allow the simulated IJPANs to take on states between approximately [-8,8] V, as indicated in Fig. 4. Otherwise, the neurons would have too much excitation energy to contain the separability needed to hyper-dimensionalize the input. In future works, automated optimization will replace manual variable selection for best IJPAN ESN performance.

B. IJP ESN Performance Results

The images are all a 28x28 matrix for a total of 784 pixels ranging from [0,1]. Each reservoir holds 200 neurons to represent a single sheet of sparsely-connected IJPANs. It is well-established that sparsely connected reservoirs reduces memory and computing power without any significant change to the prediction rates, thus making 10% connection sparsity effective at increasing training speeds. Adding Gaussian noise with a Signal-to-Noise Ratio (SNR) of 10 was found to produce best performances, as it injects enough uncertainty to make the network more robust against each image's natural variations (Fig. 7). Fig. 8a shows the modeled IJPAN's states as the reservoir updates each time-step. The output is between [-8,8] V, which is the IJPAN output range seen in the current-controlled I-V curve (Fig. 4).

TABLE I
LIST OF GLOBAL PARAMETERS FOR THE MODIFIED ESN.

Parameter	Value
Number of Epochs	40
Number of Classes	10
Train/Test Samples per Epoch	10000
Train/Test Split	80% / 20%
Number of Neurons per Reservoir	200
Number of Parallel Reservoirs	1
Input Weight Scaling	8e-11
Spectral Radius	1e-8
Learning Rate	0.05
Number of Reservoir Updates	40
Regularization (β)	1
Gaussian Noise (SNR)	10
Connectivity of the Reservoirs	10%

Given that the numerous global parameters of this ESN were manually tuned in this work, classification rates of the modified ESN for time independent inputs are lower than what optimization process will achieve. Regardless, competitive prediction rates can be visualized by the average error plot (Fig. 8b) and confusion matrix of Fig. 9. Along the x-axis, the digits 0,1,...,9 are shown as a set of 10 classes. Correct classifications are shown along the diagonal in the green boxes and incorrect classes are shown in the red boxes. The bottom right corner shows the overall classification rate of 86.2% and along the x-axis the performance for each digit is written as percentages (green text for correct classification, red text for the error rate). The digit 4 was correctly classified the least at 67.5%, most commonly mistaken as a 2. Digit 0 was recognized by the ESN more than any other digit at 98.6%.

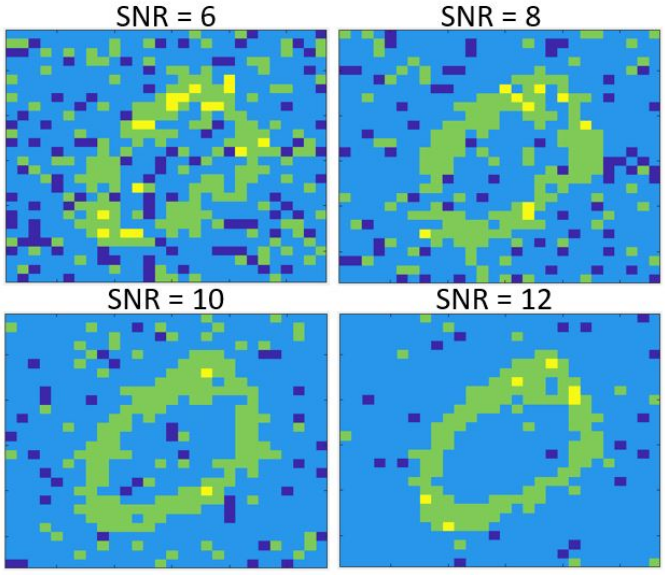

Fig. 7. Guassian noise injected into the input images as visualized at different Signal-to-Noise Ratio values.

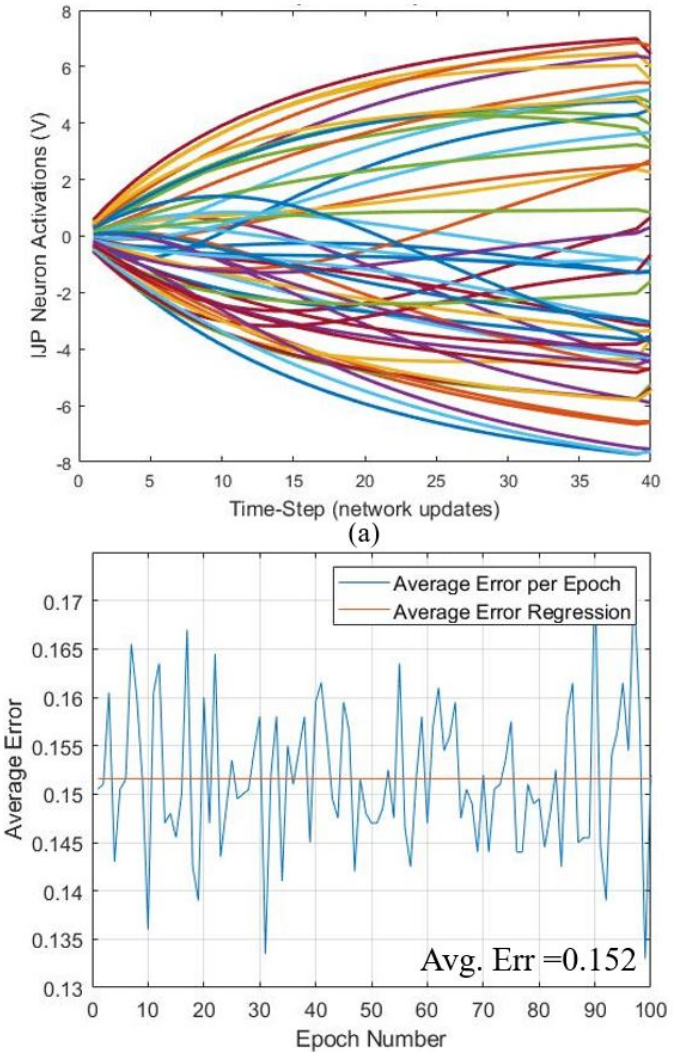

Fig. 8. (a) Visualization of the neuron states over the updates shows output between [-8,8] volts, which is the IJPAN output range seen in the current-controlled I-V curve. (b) The average classification error using the IJP artificial neuron model and 200 neurons is 15.2%.

Training and image processing time are particularly important when image processing speed is the most critical factor. For 10,000 train/test digits with the values in Table I, the entire training time is 14 minutes. The contents of Table II shows the overall error rate and training times for different artificial neuron types in the mESN. In each case, the total number of IJPANs remains the same at 200.

VI. Results and Discussions

A. IJPAN Behavior

The viability of this IJP artificial neuron is clear based on the results of the work, where classification performance is equal to or marginally better than the standard sigmoid and hyperbolic tangent activation functions. Fabrication of each IJPAN will have varied behaviors, but can have improved reliability and operating bias consistency with a standardized protocol and electrical quality checks. Over 16 samples were tested, and all obtained the same non-linear profile. However, the current biases were different depending on the variation in nanoparticle dispersion during curing. The hBN and GN were applied by precision pipette, but still have variation from it being ejected by hand. Thus, Eq. 4 represents the non-linear behavior of a single element for modeling. For more consistent samples, plans are in place to utilize the V-One PCB Printer to disperse the hBN and GN far more precisely. The price of each IJPAN is estimated to be $0.02 and thus having some poor-quality neurons is not monetarily detrimental. The output voltage range is tuned based on the density of graphene nanoparticles in the channel region, with less density resulting in less current flow and higher voltage across terminals (and vice versa). High voltages can be generated with little active material layering and may be considered as a method of driving voltage-controlled IJP elements requiring high-voltages.

TABLE II
Best mESN performances of standard activation functions compared to the modeled IJPAN.

Metric	sigmoid(x)	tanh(x)	IJPAN
Avg. Class. Rate (%)	86.1	87.2	**88.1**
Avg. Train Time/Epoch (s)	25.7	25.9	29.3
Avg. Image Class. Time (ms)	4.04	4.23	9.69

B. IJPAN-ESN Performance

Performances are approximately the same, as indicated in Table II. Using a function that acts as a standard hyperbolic tangent but does not saturate works similarly to the original

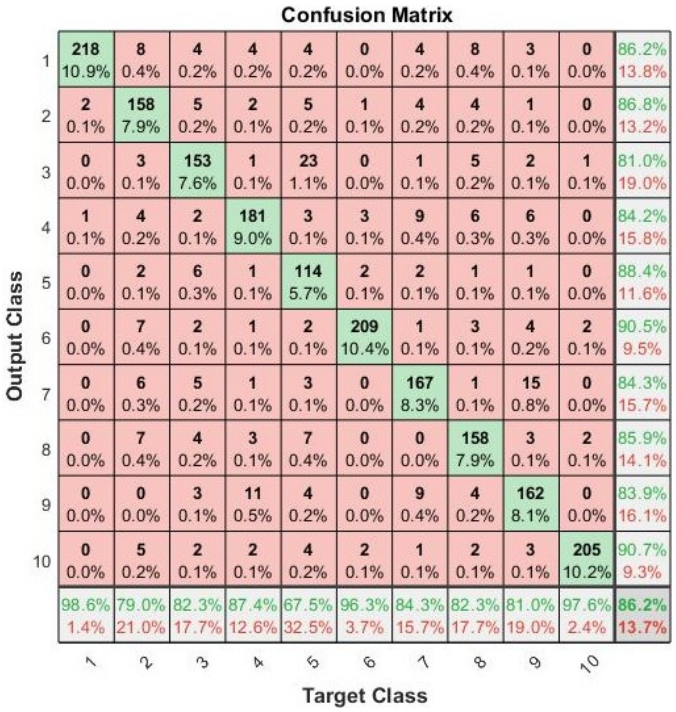

Fig. 9. Confusion matrix of the modified ESN-based classification model. The matrix shows the desired output digit along the x-axis and the ESN output classification along the y-axis. The diagonal (green) shows the correctly classified digits, with overall error rate in the bottom right corner. The error rates of each digit can be seen along the x-axis.

activation function. However, it has not been proven in this work to significantly improve classification rates. The low spectral radius of the ESN (Table I) is an indication that the network is not relying much on its memory to classify the handwritten digits, which is expected for the time-invariant inputs. Instead, an optimized minimum cost gradient is calculated and the output weights are updated. The higher processing time of the IJPAN was mainly due to the software-level custom function definition, as compared to the standard sigmoid and tanh equations which are less computationally expensive. However, the IJP neural network is targeted to be analog, and published work done on this element adapted as a touch sensor shows nearly instantaneous response times [42]. Its output would be a set of non-linear states and the software-level function is no longer needed and power/processing time are conserved. The results of this work add to mounting evidence that the ESN, even with a physical reservoir, can be used to classify time-invariant inputs.

C. Physical IJPAN Network Considerations

Forming a physical IJP neural network is a greater challenge to consider since (1) the reservoir weights must be within a proper spectral radius, (2) have adequate and random connections, and (3) have the power through-put to operate. Addressing (1) will require post-processing where the coupling weights of the reservoir are used to calculate the proper spectral radius. For challenge (2), the natural variability between fabricated samples of the IJPANs along with inclusion of IJP resistors will form the reservoir weight matrix, the values of which being collected as a set of resistances. For challenge (3), several connection topologies such as star, grid, ring, etc. can be considered for minimized power utilization while maintaining a strong non-linear network.

A critical shortfall of most IJP electronics is their operating lifetime and reliability, as they degrade based on environmental conditions and tactile wear. Thus, the IJPAN operating biases will drift according to those variables, altering the spectral radius of the physical reservoir. Mitigating the signal changes can be done by applying proper protective layers. To ensure the reservoir operates, an adaptive spectral radius may be included where the reservoir weight matrix is obtained each training cycle, the length of which being determined by studying the element's lifetime and long-term signal behaviors. Since training the ESN takes 1-2 minutes, it may be quickly retrained on the new reservoir weight matrix as a calibration technique.

Only 200 neurons were used to simplify the design to a single sheet of PET film. However, classification response will dramatically reduce given more neurons. For instance, having 4 sheets of PET film in parallel, each with 200 IJPANs, a total of 800 IJP neurons are used, increasing the average classification rate to 91%. Defining the weight connections between each coupled neuron will be another challenge to overcome, as independently testing each to fit a model and then extracting the coupling factors may be time or energy consuming. In that case, other IJP neural network topologies may be considered, such as relying on only a small number of neurons to classify, reading neuron states as a summation of the rows, or simplifying the neuron connectivity architecture.

VII. Conclusion and Future Works

New materials that have unique and chaotic properties are being explored for their abilities to compute as an alternative to existing transistors. This work shows an inkjet printed artificial neuron made from two parallel Ag terminals layered with hBN, cut to make a well, and then bridged together with GN nanoparticle ink. The device works closely to a hyperbolic sine when controlled by voltage but is the inverse hyperbolic sine when current-controlled. The IJP neuron activation function does not saturate or explode, is sufficiently non-linear, and performs similarly to the standard sigmoid and hyperbolic tangent functions. A model was fit to empirical voltage data collected from the current-controlled IJP neuron and reached a 99.7% goodness of fit. The modified ESN established in prior works had its neurons replaced with the modeled equation and trained to the MNIST benchmark dataset. Classification performances average 84.8% over 100 trials, which may be improved with network optimization. Progression of this work may lead to an IJP-CMOS ESN, where the physical reservoir is inkjet printed, becoming one of the first printed and flexible neural network prototypes. This research is highly applicable to sensor signal processing at the edge, where irregular surfaces, large-areas, and ultra-thin profiles are requirements. Signals in need of interpretation, classification, or prediction benefit from this work (e.g. wearable telehealth sensor signal processing, multi-scale sensor network fault detection, environmental sensing/monitoring, etc.).

The performance of the modified ESN is highly dependent on spectral radius, input scaling, and number of parallel reservoirs, but changing any of the variables affects the system enough to make its robustness an area in need of improvement. This obviates the need for hyperparameter optimization, which is a part of our future planned research. There are many components of the ESN in this work that will be modified for better performance. Data augmentation will include translating and rotating images instead of just injecting noise. For more complex datasets, feature extraction will be performed prior to running the ESN for more enriched data. Series (i.e. deep) IJPAN reservoirs can be implemented to images that are time independent in a more meaningful manner since memory capacity has less impact in those tests. The read-out layer will be replaced with a more robust feed-forward network like the multilayer perceptron (MLP). With respect to the IJPAN, a study of lifetime, variability, and fabrication approaches will give insight to its requirements for physical implementation as described in the discussion.

This work has shown that a network of modeled IJPAN's can perform similarly to existing sigmoid and tangent artificial neurons, and may be eventually implemented as an analog neural network that is an energy efficient alternative to CMOS neural networks.

VIII. Acknowledgment

This research was partially supported by Army Research Center Phase V – Cooperative Agreement No.1.A83 (Federal Award No. W56HZV-19-2-0001), and National Science Foundation (Award No. ECCS-1813949). However, any

opinions, findings, conclusions, or recommendations expressed herein are those of the authors and do not necessarily reflect the views of the funding agencies. The authors also thank Mr. Muhammad Masud Rana for his help preparing the draft.

REFERENCES

[1] P. Ye, T. Ernst, and M. Khare, "The last silicon transistor: Nanosheet devices could be the final evolutionary step for moore's law," *IEEE Spectrum*, vol. 56, pp. 30–35, 08 2019.

[2] C. Sung, H. Hwang, and I. K. Yoo, "Perspective: A review on memristive hardware for neuromorphic computation," *Journal of Applied Physics*, vol. 124, no. 15, 2018.

[3] M. Ziegler, C. Wenger, E. Chicca, and H. Kohlstedt, "Tutorial: Concepts for closely mimicking biological learning with memristive devices: Principles to emulate cellular forms of learning," *Journal of Applied Physics*, vol. 124, no. 15, 2018.

[4] Y. Halawani, B. Mohammad, D. Homouz, M. Al-Qutayri, and H. Saleh, "Modeling and optimization of memristor and stt-ram-based memory for low-power applications," *IEEE Transactions on Very Large Scale Integration (VLSI) Systems*, vol. 24, no. 3, pp. 1003–1014, 2016.

[5] H. Al-Bustami, G. Koplovitz, D. Primc, S. Yochelis, E. Capua, D. Porath, R. Naaman, and Y. Paltiel, "Single nanoparticle magnetic spin memristor," *Small*, vol. 14, no. 30, 2018.

[6] D. Fan, M. Sharad, and K. Roy, "Design and synthesis of ultralow energy spin-memristor threshold logic," *IEEE Transactions on Nanotechnology*, vol. 13, no. 3, pp. 574–583, 2014.

[7] D. Fan, M. Sharad, A. Sengupta, and K. Roy, "Hierarchical temporal memory based on spin-neurons and resistive memory for energy-efficient brain-inspired computing," *IEEE Transactions on Neural Networks and Learning Systems*, vol. 27, no. 9, pp. 1907–1919, 2016.

[8] J. Hillier, K. Ibukuro, F. Liu, M. H. Khaled, J. Byers, H. N. Rutt, I. Tomita, Y. Tsuchiya, and S. Saito, "Investigating stability and tunability of quantum dot transport in silicon MOSFETs via the application of electrical stress," *Journal of Physics D: Applied Physics*, vol. 55, no. 10, p. 105107, Dec 2021.

[9] Z. Dong, D. Qi, Y. He, Z. Xu, X. Hu, and S. Duan, "Easily cascaded memristor-cmos hybrid circuit for high-efficiency boolean logic implementation," *International Journal of Bifurcation and Chaos*, vol. 28, no. 12, 2018.

[10] G. Liu, L. Zheng, G. Wang, Y. Shen, and Y. Liang, "A carry lookahead adder based on hybrid cmos-memristor logic circuit," *IEEE Access*, vol. 7, pp. 43 691–43 696, 2019.

[11] K. V. Pham and K. Min, "Non-ideal effects of memristor-cmos hybrid circuits for realizing multiple-layer neural networks," in *2019 IEEE International Symposium on Circuits and Systems (ISCAS)*, Conference Proceedings, pp. 1–5.

[12] M. D. Bishop, G. Hills, T. Srimani, C. Lau, D. Murphy, S. Fuller, J. Humes, A. Ratkovich, M. Nelson, and M. M. Shulaker, "Fabrication of carbon nanotube field-effect transistors in commercial silicon manufacturing facilities," *Nature Electronics*, vol. 3, no. 8, pp. 492–501, 2020.

[13] Y. Luo, M. Wang, C. Wan, P. Cai, X. J. Loh, and X. Chen, "Devising materials manufacturing toward lab-to-fab translation of flexible electronics," *Advanced materials (Weinheim)*, vol. 32, no. 37, pp. 2 001 903–n/a, 2020.

[14] V. V. Soman, Y. Khan, M. Zabran, M. Schadt, P. Hart, M. Shay, F. D. Egitto, K. I. Papathomas, N. A. D. Yamamoto, D. Han, A. C. Arias, K. Ghose, M. D. Poliks, and J. N. Turner, "Reliability challenges in fabrication of flexible hybrid electronics for human performance monitors: A system-level study," *IEEE Transactions on Components, Packaging and Manufacturing Technology*, vol. 9, no. 9, pp. 1872–1887, 2019.

[15] W. Cui, W. Lu, Y. Zhang, G. Lin, T. Wei, and L. Jiang, "Gold nanoparticle ink suitable for electric-conductive pattern fabrication using in ink-jet printing technology," *Colloids and Surfaces A: Physicochemical and Engineering Aspects*, vol. 358, no. 1-3, pp. 35–41, 2010.

[16] T. Yun, S. Eom, and S. Lim, "Paper-based capacitive touchpad using home inkjet printer," *Journal of Display Technology*, vol. 12, no. 11, pp. 1411–1416, 2016.

[17] M. Borghetti, E. Sardini, and M. Serpelloni, "Preliminary study of resistive sensors in inkjet technology for force measurements in biomedical applications," in *2014 IEEE 11th International Multi-Conference on Systems, Signals & Devices (SSD14)*, Conference Proceedings, pp. 1–4.

[18] B. Andò, S. Baglio, C. O. Lombardo, and V. Marletta, "An inkjet printed sensor for load measurement," in *2014 IEEE Sensors Applications Symposium (SAS)*, Conference Proceedings, pp. 185–188.

[19] P. Branchini, A. Fabbh, D. Riondino, L. Mariucci, M. Rapisarda, A. Valletta, A. Aloisio, and F. D. Capua, "Logic gates and memory elements design and simulation using pmos organic transistor," in *2017 IEEE 26th International Symposium on Industrial Electronics (ISIE)*, Conference Proceedings, pp. 2097–2101.

[20] Y. Fang, X. Wu, S. Lan, J. Zhong, D. Sun, H. Chen, and T. Guo, "Inkjet-printed vertical organic field-effect transistor arrays and their image sensors," *ACS Applied Materials and Interfaces*, vol. 10, no. 36, pp. 30 587–30 595, 2018.

[21] G. M. Tornez Xavier, F. Gómez Castañeda, L. M. Flores Nava, and J. A. Moreno Cadenas, "Memristive recurrent neural network," *Neurocomputing*, vol. 273, pp. 281–295, 2018.

[22] H. Jaeger, "Short term memory in echo state networks." *German National Research Institute for Computer Science*, vol. GMD-Report 152, 2012.

[23] W. Maass, T. Natschlager, and H. Markram, "Real-time computing without stable states: A new framework for neural based on perturbations," *Neural Computation*, vol. 14, p. 2531–2560, 2002.

[24] Z. Zhao, A. Srivastava, L. Peng, and Q. Chen, "Long short-term memory network design for analog computing," *ACM Journal on Emerging Technologies in Computing Systems (JETC)*, vol. 15, no. 1, pp. 1–27, 2019.

[25] Y. Kume, S. Bian, and T. Sato, "A tuning-free hardware reservoir based on mosfet crossbar array for practical echo state network implementation," in *2020 25th Asia and South Pacific Design Automation Conference (ASP-DAC)*, 2020, pp. 458–463.

[26] H. Jaeger, "A tutorial on training recurrent neural networks, covering bppt, rtrl, ekf and the "echo state network" approach," *Fraunhofer Institute for Autonomous Intelligent Systems (AIS)*, vol. GMD Report 159, 2002.

[27] H. Jaeger, W. Maass, and J. Principe, "Special issue on echo state networks and liquid state machines," *Neural Networks*, vol. 20, no. 3, pp. 287–289, 2007.

[28] W. Maass, T. Natschlager, and H. Markram, *Computational Models for Generic Cortical Microcircuits*. CRC-Press, 2002, book section 149.

[29] W. Maass and H. Markram, "On the computational power of circuits of spiking neurons," *Elsevier Science*, 2004.

[30] M. L. Alomar, M. C. Soriano, M. Escalona-Morán, V. Canals, I. Fischer, C. R. Mirasso, and J. L. Rosselló, "Digital implementation of a single dynamical node reservoir computer," *IEEE Transactions on Circuits and Systems II: Express Briefs*, vol. 62, no. 10, pp. 977–981, 2015.

[31] K. Bai and Y. Y. Bradley, "A path to energy-efficient spiking delayed feedback reservoir computing system for brain-inspired neuromorphic processors," in *2018 19th International Symposium on Quality Electronic Design (ISQED)*, Conference Proceedings, pp. 322–328.

[32] S. D. Gardner, M. R. Haider, L. Moradi, and V. Vantsevich, "A modified echo state network for time independent image classification," in *2021 IEEE International Midwest Symposium on Circuits and Systems (MWSCAS)*, 2021, pp. 255–258.

[33] Y. LeCun, C. Cortes, and C. J. Burges, "The mnist database of handwritten digits," *The Courant Institute of Mathematical Sciences, NYU Google Labs, New York Microsoft Research, Redmond*, 2012.

[34] L. Manneschi, M. O. A. Ellis, G. Gigante, A. C. Lin, P. Del Giudice, and E. Vasilaki, "Exploiting multiple timescales in hierarchical echo state networks," *Frontiers in Applied Mathematics and Statistics*, vol. 6, no. 76, 2021.

[35] N. Schaetti, M. Salomon, and R. Couturier, "Echo state networks-based reservoir computing for mnist handwritten digits recognition," *International Conference on Computational Science and Engineering*, 2016.

[36] I. Goodfellow, Y. Bengio, and A. Courville, *Deep Learning*. The MIT Press, 2016.

[37] Y. Li, Y. Lin, M. Madhusudan, A. Sharma, W. Xu, S. Sapatnekar, R. Harjani, and J. Hu, "Exploring a machine learning approach to performance driven analog ic placement," in *2020 IEEE Computer Society Annual Symposium on VLSI (ISVLSI)*, 2020, pp. 24–29.

[38] T. Chen, J. v. Gelder, B. v. d. Ven, H.-C. R. Euler, H. Broersma, W. G. v. d. Wiel, S. V. Amitonov, P. A. Bobbert, B. d. Wilde, and F. A. Zwanenburg, "Classification with a disordered dopantatom network in silicon," *Nature*, vol. 577, 2020.

[39] X. Glorot, A. Bordes, and Y. Bengio, "Deep sparse rectifier neural networks," in *Proceedings of the Fourteenth International Conference on Artificial Intelligence and Statistics*, ser. Proceedings of Machine Learning Research, G. Gordon, D. Dunson, and M. Dudík, Eds., vol. 15. Fort Lauderdale, FL, USA: PMLR, 11–13 Apr 2011, pp. 315–323.
[40] A. Souahlia, A. Belatreche, A. Benyettou, Z. Ahmed-Foitih, E. Benkhelifa, and K. Curran, "Echo state network-based feature extraction for efficient color image segmentation," *Concurrency and Computation: Practice and Experience*, vol. 32, no. 21, 2020.
[41] M. Lukosevicius, *A Practical Guide to Applying Echo State Networks*. Springer, 2012, vol. 7700, p. 659–686.
[42] S. D. Gardner, J. I. D. Alexander, Y. Massoud, and M. R. Haider, "An inkjet-printed paper-pased flexible sensor for pressure mapping applications," *IEEE International Symposium on Circuits and Systems (ISCAS)*, 2020.

IX. Author Biographies

Steven D. Gardner is a graduate researcher and Ph.D. candidate at the University of Alabama at Birmingham (UAB) in the Electrical and Computer Engineering department, located in Birmingham, AL, US. He obtained a B.S. Electrical Engineering from Auburn University in 2016 and a M.S. Electrical and Computer Engineering from UAB in 2018, where he was named Graduate Student of the Year by UAB School of Engineering. Mr. Gardner has expertise with flexible and non-silicon electronics, and a special focus on inkjet-printed technologies, sensors, and circuits. Alternative computing, neuromorphics, and analog neural networks for signal processing are his primary research topics, although his merits extend to Internet-of-Things telehealth devices, autonomous vehicle perception, civil structure deformation monitoring, electrical power systems, photovoltaics, and more. Mr. Gardner is published in over 10 works related to inkjet-printed sensors/circuits and Echo State Networks and actively contributes to this field of research.

Mohammad R. Haider received his B.Sc. and M.Sc. degrees in 2002 and 2004, respectively, from Bangladesh University of Engineering and Technology (BUET), the top ranked engineering university in Bangladesh. He received his PhD degree in Electrical and Computer Engineering from the University of Tennessee at Knoxville in 2008. He is currently an Associate Professor in the department of Electrical and Computer Engineering with the University of Alabama at Birmingham (UAB). Dr. Haider also served in the Sonoma State University from 2009 to 2010. Dr. Haider's research interests are in the areas of design, simulation, and experimental validation of low-power analog and radio-frequency integrated circuits and systems for the short-range wireless telemetry, energy-efficient neuromorphic circuits and systems, machine learning for sensors and systems, analog orthogonal pulse-based spectrum-efficient high-density wireless data telemetry, and inkjet-printed nanoparticle-based flexible sensors and electronics for in-situ alternative computing. He has authored more than 120 (one hundred twenty) articles in international journals and conference proceedings. He has been serving as an Associate Editor of Microelectronics Journal, Academic Editor of Journal of Sensors, and Editorial Board Member of Journal of Low Power Electronics and Applications. He has also served as the reviewers of several internal journals and conferences, Technical Program Committee Members, Track Chairs, and Sessions Chairs of IEEE International Symposium on Smart Electronic Systems (iSES) 2021, IEEE International System-on-Chip Conference (SOCC) 2019, IEEE International Midwest Symposium on Circuits and Systems (MWSCAS) 2018, IEEE International Symposium of Circuits and Systems (ISCAS) 2020, IEEE International Midwest Symposium on Circuits and Systems (MWSCAS) 2021, IEEE SoutheastCon 2022. Dr. Haider also co-authored one book entitled "Sensors and Low-Power Signal Processing" ISBN: 978-0-387-79391-7, two book chapters, and three patent disclosers. His works have been supported by National Science Foundation (NSF), National Cooperative Highway Research Program (NCHRP), US Army, and local agencies.